Monthly Notices of the ROYAL ASTRONOMICAL SOCIETY

MNRAS **534,** L35–L41 (2024) https://doi.org/10.1093/mnrasl/slae077
Advance Access publication 2024 August 12

Magnesium isotope ratios in Milky Way and dwarf galaxy stars

M. McKenzie [1,2]★ S. Monty [3] D. Yong [1,2] C. Kobayashi [4] A. I. Karakas [2,5] P. E. Nissen,[6] J. E. Norris,[1] A. Rains [7] A. Mura-Guzmán [1,2] E. X. Wang [1,2] and S. Martell [2,8]

[1]*Research School of Astronomy & Astrophysics, Australian National University, Canberra, ACT 2611, Australia*
[2]*ARC Centre of Excellence for Astrophysics in Three Dimensions (ASTRO-3D), Canberra, ACT 2611, Australia*
[3]*Institute of Astronomy, University of Cambridge, Madingley Road, Cambridge CB3 0HA, UK*
[4]*Centre for Astrophysics Research, Department of Physics, Astronomy and Mathematics, University of Hertfordshire, Hatfield AL10 9AB, UK*
[5]*School of Physics & Astronomy, Monash University, Clayton, VIC 3800, Australia*
[6]*Department of Physics and Astronomy, Aarhus University, Ny Munkegade 120, DK-8000 Aarhus C, Denmark*
[7]*Department of Physics and Astronomy, Uppsala University, Box 516, SE-75120 Uppsala, Sweden*
[8]*School of Physics, University of New South Wales, Sydney, NSW 2052, Australia*

Accepted 2024 July 25. Received 2024 July 4; in original form 2024 April 14

ABSTRACT

Under the assumption of hierarchical galaxy formation, dwarf galaxies are the closest existing analogues to the high-redshift protogalaxies that merged to form the Milky Way. These low-mass systems serve as unique laboratories for studying nucleosynthetic channels given that the chemical compositions of their stars play a pivotal role in constraining their chemical enrichment history. To date, stellar abundances in dwarf galaxies have focused almost exclusively on elemental abundance ratios. While important, elemental abundances omit critical information about the isotopic composition. Here, we compute the Mg isotopic ratios of six accreted dwarf galaxy stars (low α) and seven Milky Way stars (high α) using a set of high-resolution ($65\,000 < R < 160\,000$) and high signal-to-noise ratio (S/N > 250) optical spectra. We show, for the first time, that at a given [Fe/H] stars born in a dwarf galaxy differ in their Mg isotopic ratios from stars born in the Milky Way. However, when comparing isotopic ratios at a given [Mg/H] rather than [Fe/H], a powerful diagnostic emerges that suggests nucleosynthesis processes are consistent across different stellar environments. This universality of Mg isotopic abundances provides additional dimensionality for chemical evolution models and helps to constrain massive star nucleosynthesis across cosmic time.

Key words: nuclear reactions, nucleosynthesis, abundances – techniques: spectroscopic – stars: abundances – stars: kinematics and dynamics – Galaxy: evolution.

1 INTRODUCTION

Although small in mass, dwarf galaxies have had an enormous impact on our understanding of the Universe. As the building blocks of galaxies we see today and closest existing analogues to high-redshift protogalaxies, dwarf galaxies play a critical role in understanding the grand narrative of cosmic history and hierarchical formation (e.g. Madau et al. 1996; Mateo 1998; Moore et al. 1999; McConnachie 2012; Bullock & Boylan-Kolchin 2017).

Lambda cold dark matter cosmology predicts that galaxies grow through a series of merger events, as shown in cosmological simulations (e.g. Springel et al. 2005; Vogelsberger et al. 2014; Schaye et al. 2015). Within our own Galaxy, significant progress has been made in characterizing the various components of the accreted halo of the Milky Way (MW; e.g. Belokurov et al. 2018; Haywood et al. 2018; Helmi et al. 2018; Matsuno, Aoki & Suda 2019; Myeong et al. 2019; Monty et al. 2020; Yuan et al. 2020; Feuillet et al. 2021; Horta et al. 2021, 2023; Naidu et al. 2021; Dodd et al. 2023). The ongoing disruption of the Sagittarius dwarf spheroidal galaxy (Ibata, Gilmore & Irwin 1994; Davies et al. 2024) and the large number of tidal streams (Helmi et al. 1999; Belokurov et al. 2006; Shipp et al. 2018; Ji et al. 2020) reinforce the hierarchical nature of galaxy formation and the key role dwarf galaxies play in this process.

Chemical abundance ratios provide a valuable tool for understanding the star formation history (SFH) of a galaxy (Wallerstein 1962; Tinsley 1979; Bensby et al. 2005). In particular, the mean [α/Fe] ratio[1] assesses the contribution from massive stars with short lifetimes that die as core-collapse supernovae (CCSNe), largely producing α elements with modest amounts of Fe, and longer lived thermonuclear supernovae [Type Ia supernovae (SNe Ia)] that dominate the production of Fe-peak elements (Matteucci & Greggio 1986; Woosley & Weaver 1995; Thielemann, Nomoto & Hashimoto 1996; Kobayashi, Leung & Nomoto 2020a; Kobayashi, Karakas & Lugaro 2020b).

Additionally, the evolution of [α/Fe] with metallicity below the α-knee reveals insights into pre-SNe Ia star formation efficiency. In the [Fe/H] > -3 regime, dwarf galaxies typically show lower α

[1]Where α represents elements produced via the α process, such as O, Mg, and Si.

★ E-mail: madeleine.mckenzie@anu.edu.au

abundances compared to the MW, likely due to differing SFHs (Venn et al. 2004; Tolstoy, Hill & Tosi 2009). Galactic chemical evolution models have been used to interpret SFHs in the MW and Local Group dwarf galaxies (e.g. Kobayashi et al. 2020a; Hasselquist et al. 2021). However, these models are sensitive to predictions of chemical yields from the various nucleosynthetic channels (Romano et al. 2010; Côté et al. 2017).

Nissen & Schuster (2010, hereafter NS10, 2011) identified high- and low-[α/Fe] populations of halo stars in the solar neighbourhood and attributed the appearance of the two sequences to the existence of *in situ* and accreted components in the MW halo. Specifically, the high-α population is indicative of efficient star formation in the early MW, while the low-α population was likely accreted from dwarf galaxies that experienced less efficient star formation. Today, the majority of the low-α component is attributed to the Gaia-Sausage-Enceladus (GSE) accretion event (Belokurov et al. 2018; Haywood et al. 2018; Helmi et al. 2018), presumed to have occurred $\sim$10 Gyr ago, and dominates the population of halo stars below [Fe/H] < -1.5. The high-α sequence discovered in NS10 is likely connected to the population of 'Aurora' and 'Splash' stars discussed in Belokurov et al. (2020) (see also Bonaca et al. 2017; Gallart et al. 2019). Aurora is likely an ancient portion of the MW that existed prior to the formation of the disc and has low metallicities and low tangential velocities, whereas Splash stars can be found at higher metallicities than both GSE and Aurora but display a range of tangential velocities in addition to a net rotation.

The bright accreted stars from the NS10 sample offer an unparalleled opportunity to not only quantify chemical compositions in terms of overall abundances but also understand how the elements are distributed among their constituent isotopes. Although 'isotopic analysis is one of the most difficult sub-fields of spectroscopic astronomy' (Shetrone 1996), it offers the most direct insight into nucleosynthesis and chemical enrichment (e.g. Kobayashi, Karakas & Umeda 2011). Applications of isotopic measurements include CNO isotopic ratios for the interstellar medium (e.g. Romano et al. 2019), C isotopic ratios in stars (e.g. Spite et al. 2006), and Li isotopic ratios to probe big bang nucleosynthesis (e.g. Fields 2011; Wang et al. 2022).

The relative abundances of ^{24}Mg, ^{25}Mg, and ^{26}Mg can be quantified via asymmetries in MgH molecular lines at around 5100 Å. The dominant α-nucleus ^{24}Mg is synthesized during C and Ne burning in massive stars. Conversely, the production of the rarer neutron-rich isotopes ^{25}Mg and ^{26}Mg occurs during helium burning in massive stars ($\gtrsim$8 M$_\odot$) as well as during helium-shell burning in intermediate-mass (3–8 M$_\odot$) asymptotic giant branch (AGB) stars (Karakas & Lattanzio 2003). The isotopic yields from CCSNe are also metallicity dependent (Kobayashi et al. 2011) and potentially offer a more refined SFH 'clock' than elemental abundances alone. Unfortunately, even with efficient modern spectrographs on 8–10 m class telescopes, the exposure times required for Mg isotopic analysis in surviving dwarf galaxy stars are impractical.

Pioneering studies of Mg isotopes iteratively fit synthetic spectra to individual MgH lines by hand (Boesgaard 1968; Bell et al. 1970; Tomkin & Lambert 1976, 1980; Barbuy 1985, 1987; Barbuy, Spite & Spite 1987; McWilliam & Lambert 1988; Gay & Lambert 2000). Subsequent studies improved upon this by applying a grid-based search for the best-fitting spectra over a small number of parameters to recover the isotopic ratios (Yong et al. 2003a, 2004, 2008; Yong, Lambert & Ivans 2003b; Yong, Aoki & Lambert 2006; Meléndez & Cohen 2007, 2009; Da Costa, Norris & Yong 2013; Thygesen et al. 2016; Carlos et al. 2018). Recently, McKenzie et al. (2024) developed a powerful new tool capable of determining isotopic ratios based on more than three times the number of MgH lines previously used. This tool also takes several additional parameters into account, such as macroturbulent velocity and continuum placement, and assigns realistic errors to the isotopic ratios for the first time.

In this letter, we present measurements of Mg isotope ratios in low-α accreted dwarf galaxy stars to reveal details of massive star contributions that cannot be learnt from element abundances alone. In Section 2, we describe our observations and analysis; in Section 3, we discuss our results; and in Section 4, we present our conclusions.

2 OBSERVATIONS AND ANALYSIS

2.1 Target selection and observations

We analyse 13 targets in this letter. Six targets were observed using the Ultraviolet and Visual Echelle Spectrograph (UVES) instrument at the Very Large Telescope (VLT; Dekker et al. 2000) with image slicer #3 and a 0.3 arcmin slit that provided a spectral resolution of $R = 110\,000$. Four stars were observed using the High Resolution Echelle Spectrometer (HIRES; Vogt et al. 1994) at the Keck telescopes. The 0.4 arcmin slit was used that provided a spectral resolution of $R \simeq 90\,000$. Two stars were observed using the Magellan Inamori Kyocera Echelle (MIKE; Bernstein et al. 2003) at the Magellan Telescope. The 0.35 arcmin slit was used providing a spectral resolution of $R = 65\,000$. Two stars were taken with permission from Gay & Lambert (2000), observed using the 2.7-m Harlan J. Smith reflector and its Coudé spectrograph at McDonald Observatory with a spectral resolution of $R = 160\,000$. All observations have signal-to-noise ratio (S/N) ranging from 300 to 400 pixel^{-1} near the MgH lines at 5140 Å.

In Table 1, we list which instrument each star was observed with and the original reference to the data. Very few metal-poor stars with measurable MgH lines and high-quality spectra exist in the literature. However, we include as many low-α stars with MgH lines with high-resolution ($R > 60\,000$) and high-S/N (S/N $\gtrsim$ 250) spectra as are available to us.

2.2 Stellar parameters and chemical abundances

When available, stellar parameters and total Mg abundances are from NS10. For the remaining stars, we adopted the following approach. Reggiani & Meléndez (2018) presented differential stellar parameters for Gmb 1830 (HD 103095), HD 134439, HD 134440, and HD 163810. HD 163810 is also included in the NS10 sample, and therefore we shift the Reggiani & Meléndez (2018) stellar parameters and Mg abundances on to the NS10 scale ([Fe/H]$_{\rm NS10}$, [Mg/Fe]$_{\rm NS10}$). For the Keck observations, we analysed those stars differentially with respect to HD 103095 and thus on to the NS10 scale. We provide these stellar parameters and abundances in Table 1.

2.3 Mg isotopic analysis

We use the same method outlined in McKenzie et al. (2024) using our Mg isotopic analysis code RATIO.[2] The process for determining our isotopic ratios is described in detail in that work. However, we summarize it here for completeness.

We perform a routine based on Markov chain Monte Carlo optimization of the total Mg abundance, macroturbulent velocity, the ratios of ^{25}Mg/^{24}Mg and ^{26}Mg/^{24}Mg, the placement of the

[2]https://github.com/madeleine-mckenzie/RAtIO

Table 1. The stellar parameters and details of our target stars. Stellar parameters and abundances of HD 134439, HD 134 440, and HD 103 095 come from Reggiani & Meléndez (2018) and are shifted on to the abundance scale of NS10 for both [Fe/H] and [Mg/Fe] ([Fe/H]$_{NS10}$ and [Mg/Fe]$_{NS10}$, respectively). We perform our own differential abundance measurements for GJ 1064, LHS 3780, PLX 5805, and PLX 2019 and also shift them to match NS10. For G66−22, we have spectra from both the UVES and MIKE instruments.

Name	*Gaia* DR3 ID	$T_{\rm eff}$ (K)	log g (dex)	[Fe/H]	ξ (km s^{-1})	[Fe/H]$_{NS10}$	[Mg/Fe]$_{NS10}$	Instrument	Reference
G13−38	3700341138433848832	5263	4.54	−0.88	0.9	−0.88	0.35	UVES	This work
G18−28	2728314787225296000	5372	4.41	−0.83	1.0	−0.83	0.36	MIKE	Fishlock et al. (2017)
G66−22	1159108770069883136	5236	4.41	−0.86	0.9	−0.86	0.08	UVES, MIKE	This work, Fishlock et al. (2017)
G82−05	3202470247468181632	5277	4.45	−0.75	0.9	−0.75	0.06	UVES	This work
GJ 1064	231113736385994624	5136	4.54	−1.02	0.4	−0.96	0.44	HIRES	Yong et al. (2003b)
HD 103095	4034171629042489088	5100	4.65	−1.35	0.9	−1.29	0.21	McDonald	Gay & Lambert (2000)
HD 134439	6307374845312759552	5084	4.66	−1.43	1.2	−1.37	0.07	UVES	This work
HD 134440	6307365499463905536	4946	4.68	−1.39	1.2	−1.33	0.03	McDonald	Gay & Lambert (2000)
HD 222766	2439291667485442688	5334	4.27	−0.67	0.8	−0.67	0.35	UVES	This work
HD 230409	4517777421819724416	5318	4.54	−0.85	1.1	−0.85	0.30	MIKE	Fishlock et al. (2017)
LHS 3780	2615957416265170304	4908	4.74	−1.38	0.8	−1.31	0.39	HIRES	Yong et al. (2003b)
PLX 2019	3073097998492775808	4786	4.66	−1.30	0.6	−1.24	0.23	HIRES	Yong et al. (2003b)
PLX 5805	2853258035861905664	4850	4.84	−1.45	1.2	−1.40	0.15	HIRES	Yong et al. (2003b)

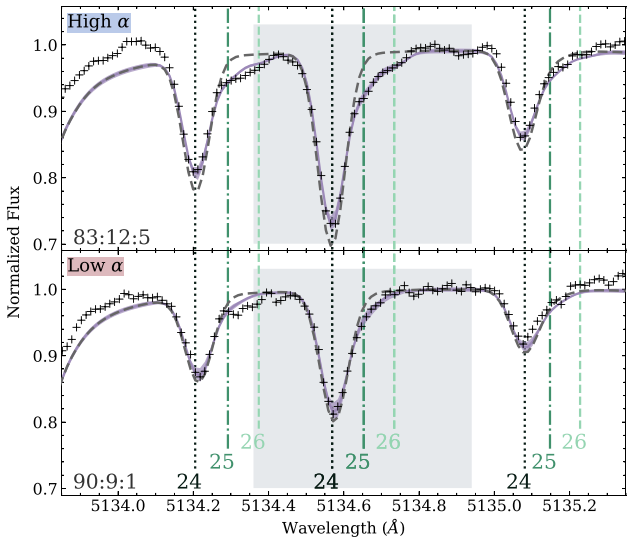

Figure 1. Two stars with similar stellar parameters both observed by the UVES instrument on the VLT: G13−38 (high α) and G66−22 (low α). The black '+' markers represent the normalized spectra, the purple line is the best-fitting model, and the grey dashed line is the best-fitting model but with only ^{24}Mg. The green vertical lines represent the location of the ^{24}Mg (dotted), ^{25}Mg (dash–dotted), and ^{26}Mg (dashed) absorption features. The bottom left corner of each panel gives the ratios for ^{24}Mg:^{25}Mg:^{26}Mg. The high-α star has a larger contribution from ^{25}Mg and ^{26}Mg, and has a deeper Mg line.

continuum, and the radial velocity correction. This acts as a wrapper for the code MOOG (Sneden 1973; Sobeck et al. 2011) and we use the 2017 version with scattering.[3]

We give an example of the fits to the 5134.6 Å line (R1 as defined in McKenzie et al. 2024) for two stars observed with UVES: G13−38 (a high-α MW star) and G66−22 (a low-α GSE star) in Fig. 1. The grey rectangle represents the χ^2 fitting region, and the purple line and shaded regions represent the best-fitting model and corresponding 16th and 84th confidence intervals, respectively. The grey dashed line gives the best-fitting model if there was only a contribution from ^{24}Mg and no ^{25}Mg or ^{26}Mg. For our high-α MW star, G13−38, there is a marked difference between the ^{24}Mg only model and our best-fitting model, illustrating the contribution from heavy Mg isotopes. The difference is far less pronounced in the low-α GSE star G66−22.

In the bottom left corner, we write the best-fitting model isotopic ratio. As we take our overall Mg isotopic ratio based on the posterior distributions of our fitting routine, the ratio for the individual line is within the error bounds of the averaged Mg isotope ratio. The neighbouring MgH features 5132.2 Å (R4) and 5135.1 Å (R5) are both well fit by the isotopic ratio found for R1, indicating a good overall fit for each star.

The original application of this code in McKenzie et al. (2024) analysed metal-poor ([Fe/H] ≈ -1.7), cool red giant branch stars, rather than the dwarfs with iron abundances in the range $-1.4 \lesssim$ [Fe/H] $\lesssim -0.7$ used in this study. We find that a larger number of MgH lines are well measured for these dwarfs compared to giants (e.g. see Table 2), leading to more robust estimates of the isotopic ratio.

2.4 Membership classification

We interpret our results in the context of the Belokurov et al. (2020) Aurora–GSE–Splash scenario for the creation of the MW halo. Membership for our stars is assigned using their integrals of motion and orbital characteristics. We integrate orbits for our sample using the orbital dynamics package GALPY (Bovy 2015) assuming the `MWPotential2014` representation of the MW potential (details of the potential components are given in table 1 of Bovy 2015). To orient ourselves, we adopt a circular velocity of 229 km s^{-1} at the solar circle (Eilers et al. 2019), assume $(U, V, W) = [11.1, 12.24, 7.25]$ km s^{-1} (Schönrich, Binney & Dehnen 2010) for the solar peculiar velocity, 8.121 kpc for the distance to the Galactic Centre (GRAVITY Collaboration 2018), and assume that the Sun is 20.8 pc above the Galactic plane in the z-direction (Bennett & Bovy 2019).

For every star in our sample, we adopt the *Gaia* Data Release 3 (DR3) proper motions and radial velocities (Gaia Collaboration 2023) and geometric distances from the Bailer-Jones et al. (2021) catalogue to build the initial 6D phase-space coordinates for the stars. The orbits are integrated forward for 2 Gyr to determine

[3] Available from https://github.com/alexji/moog17scat.

Table 2. Isotopic ratios and kinematic associations for our target stars. # lines refers to the number of lines that were used to measure the isotopic ratios (see McKenzie et al. 2024). For G66−22, we report isotopic abundances from our UVES spectra. However, these results are consistent with our MIKE spectra within our error bounds.

Name	^{25}Mg/^{24}Mg	^{26}Mg/^{24}Mg	^{24}Mg (per cent)	^{25}Mg (per cent)	^{26}Mg (per cent)	# lines	Component	Energy (km^2 s^{-2})	L_z (kpc km s^{-1})
G13−38	0.128 (±0.021)	0.061 (±0.016)	84 (±2.7)	11 (±1.5)	5 (±1.2)	6	Splash	−57 834	736
G18−28	0.158 (±0.080)	0.075 (±0.039)	81 (±7.4)	13 (±4.8)	6 (±2.5)	7	Splash	−71 841	−41
G66−22	0.063 (±0.037)	0.015 (±0.020)	93 (±4.5)	6 (±2.9)	1 (±1.6)	5	GSE	−30 935	124
G82−05	0.062 (±0.036)	0.017 (±0.019)	93 (±4.3)	6 (±2.8)	1 (±1.5)	6	GSE	−10 320	465
GJ 1064	0.148 (±0.025)	0.068 (±0.010)	82 (±2.5)	12 (±1.8)	6 (±0.7)	7	Splash	−57 683	1057
HD 103095	0.077 (±0.013)	0.008 (±0.007)	92 (±1.7)	7 (±1.1)	1 (±0.6)	6	GSE	−26 158	672
HD 134439	0.043 (±0.013)	0.008 (±0.008)	95 (±1.9)	4 (±1.2)	1 (±0.7)	7	GSE	16 051	−2200
HD 134440	0.064 (±0.007)	0.004 (±0.003)	94 (±0.9)	6 (±0.6)	0 (±0.3)	7	GSE	15 981	−2202
HD 222766	0.125 (±0.050)	0.075 (±0.030)	83 (±5.9)	11 (±3.7)	6 (±2.3)	5	Splash	−54 867	403
HD 230409	0.081 (±0.055)	0.051 (±0.027)	88 (±5.8)	7 (±3.9)	4 (±1.9)	6	Splash	−51 788	945
LHS 3780	0.070 (±0.010)	0.016 (±0.003)	92 (±1.1)	6 (±0.8)	2 (±0.3)	5	Aurora	−62 286	334
PLX 2019	0.056 (±0.008)	0.008 (±0.004)	94 (±0.9)	5 (±0.7)	1 (±0.2)	5	GSE	−42 061	−597
PLX 5805	0.057 (±0.007)	0.007 (±0.003)	94 (±0.9)	5 (±0.6)	1 (±0.2)	6	Aurora	−46 537	1079

the maximum height from the disc (z_{max}), pericentric (R_{peri}) and apocentric radii (R_{apo}), eccentricity (e), energy, and z-component of the angular momentum (L_z) directly. The actions are computed using the Stäckel 'fudge' method implemented in GALPY (Binney 2012; Mackereth & Bovy 2018). Based on our kinematic measurements, we determine that our sample contains two stars from Aurora, five from Splash, and six from GSE (see Table 2).

3 RESULTS AND DISCUSSION

3.1 Mg isotopic ratios and kinematic associations

To present our isotopic ratios and contextualize our chemodynamical associations, Fig. 2 features plots of [Mg/Fe] versus [Fe/H] (left), energy (E) versus angular momentum (middle), and action space (right). Hereafter, we use star markers to represent members of the Aurora population, plus markers for the Splash population, and squares for GSE. In the leftmost and middle panels, we show a selection of halo giants ($\log g < 2.5$) from the Apache Point Observatory Galactic Evolution Experiment (APOGEE) Data Release 17 (DR17) ALLSTAR-LITE (Abdurro'uf et al. 2022) catalogue across different metallicities and [Al/Fe]. We choose [Al/Fe] as the third dimension in Fig. 2 as it is known to be underabundant in the accreted halo (Hawkins et al. 2015), likely a reflection of inefficient star formation in the GSE dwarf.

The ALLSTAR-LITE catalogue was cleaned to remove all flagged measurements following the methodology of Belokurov & Kravtsov (2022). To select the halo sample, we keep only stars with absolute z-component of the angular momentum $|L_z| <= 3000$ km s^{-1} kpc, $z_{max} > 3$ kpc, and an azimuthal velocity $v_\phi = 80$ km s^{-1} using values from the ASTRONN APOGEE DR17 value-added catalogue (Leung & Bovy 2019a, b).[4] Following this initial cut, we redetermine the values of E and L_z for the APOGEE halo sample assuming the same frame of reference as our program stars (described in Section 2.4).

We colour our target stars by their isotopic ratio for ^{26}Mg/^{24}Mg using a green colour bar, with a lighter colour representing a larger contribution from the heavier isotope ^{26}Mg. We only show ^{26}Mg as it is less sensitive to 3D effects than ^{25}Mg based on 3D hydrodynamical modelling (Thygesen et al. 2016, 2017) and because the errors are smaller than for ^{25}Mg. However, a similar pattern emerges using ^{25}Mg. A significant result of this letter is that at metallicities greater than [Fe/H] = −1, stars formed within the GSE component have a smaller contribution from ^{26}Mg compared to their MW counterparts. One explanation is that the MW has experienced more CCSNe than GSE, thus enriching the Galaxy with heavier Mg isotopes.

[4]The apogee_astroNN-DR17.fits table is available from https://www.sdss.org/dr18/data_access/value-added-catalogs/?vac_id = 85.

3.2 Mg isotopic ratios and chemical evolution

Fig. 3 presents ^{26}Mg/^{24}Mg as a function of [Fe/H] and [Mg/H]. In the left panel, we include model predictions from Timmes, Woosley & Weaver (1995), Goswami & Prantzos (2000), and Alibés, Labay & Canal (2001), as in Yong et al. (2003b). For a description and discussion of these models, we refer the reader to Yong et al. (2003b). These models overpredict the production of ^{26}Mg/^{24}Mg at metallicities lower than [Fe/H] = −1.2, and diverge for metallicities above this. In the middle panel, we plot four different models: (1) the solar neighbourhood and (2) bulge models from Kobayashi et al. (2020b, referred to as K20 and K20 bulge, respectively) to demonstrate the dependence of the SFH; (3) the updated solar neighbourhood models with Wolf–Rayet winds (K20 + WR); and (4) models that include rotating massive star yields from Limongi & Chieffi (2018, hereafter LC18) assuming the rotational velocity distribution described in Prantzos et al. (2018). We note that the K20 + WR model uses the same yields as in Kobayashi & Ferrara (2024) for a high-redshift galaxy, while the LC18 model overproduces [(Ba, Sr, Y, Zr)/Fe] ratios (see fig. 8 of Kobayashi 2022 for 'K20 sr + rot1' and 'K20 sr + rot2', respectively).

When comparing to [Fe/H], the bulge model with a rapid star formation from K20 does an excellent job in reproducing the low-metallicity end of our measurements, with the solar neighbourhood model and solar neighbourhood models with Wolf–Rayet winds only slightly overestimating ^{26}Mg/^{24}Mg. This is consistent with the high star formation efficiency found in GSE by Hasselquist et al. (2021). The LC18 model overproduces the amount of ^{26}Mg. This is similar to results from Vangioni & Olive (2019), which also see an overestimation of ^{26}Mg when adopting LC18 models.

[Mg/H] is used in place of [Fe/H] in some galactic chemical evolution studies (e.g. Cayrel et al. 2004; Griffith, Johnson & Weinberg 2019; Griffith et al. 2022; Weinberg et al. 2022; Nissen et al. 2024) and therefore we use this as the x-axis in our rightmost

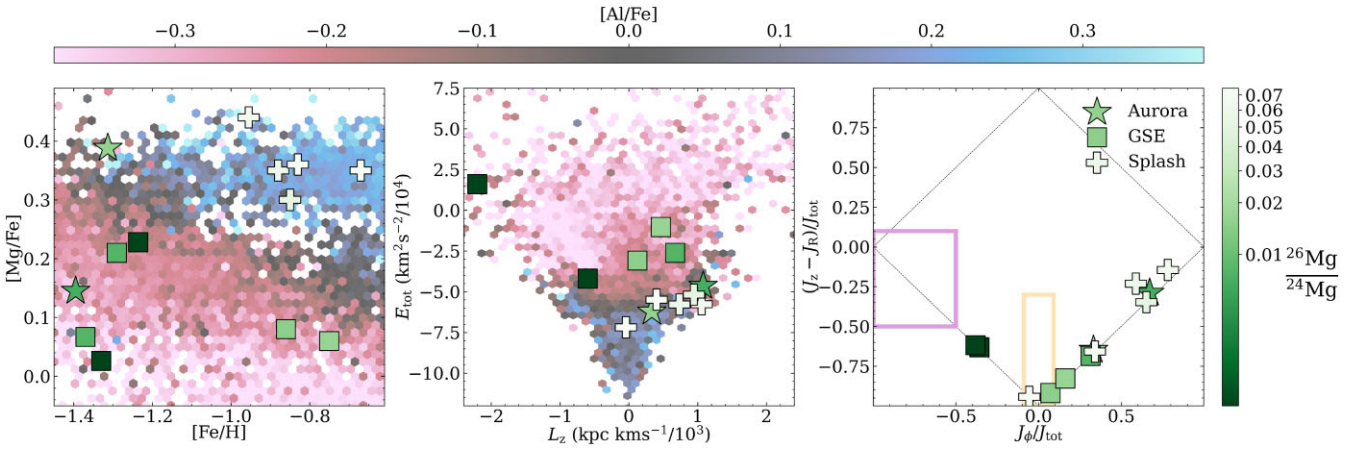

Figure 2. Membership classifications coupled with the Mg isotope ratio ^{26}Mg/^{24}Mg in terms of [Mg/Fe] against [Fe/H] (left), energy and angular momentum (middle), and action space (right). Targets belonging to the Aurora component are given as a star marker, Splash as a plus marker, and GSE as a square. The leftmost and central panels use APOGEE data binned using the `matplotlib.hexbin` function to contextualize our membership selection. In the rightmost panel, the orange rectangle at the bottom and purple rectangle to the left represent the approximate locations of the GSE and Gaia–Sequoia accretion events as given by Myeong et al. (2019) and as shown in Monty et al. (2020). We use a logarithmic colour bar for our Mg isotope ratio to better distinguish between stars with a small contribution from ^{26}Mg. HD 134440 and HD 134439 have very similar orbital parameters and sit on top of each other in the energy and angular momentum, and action space plots.

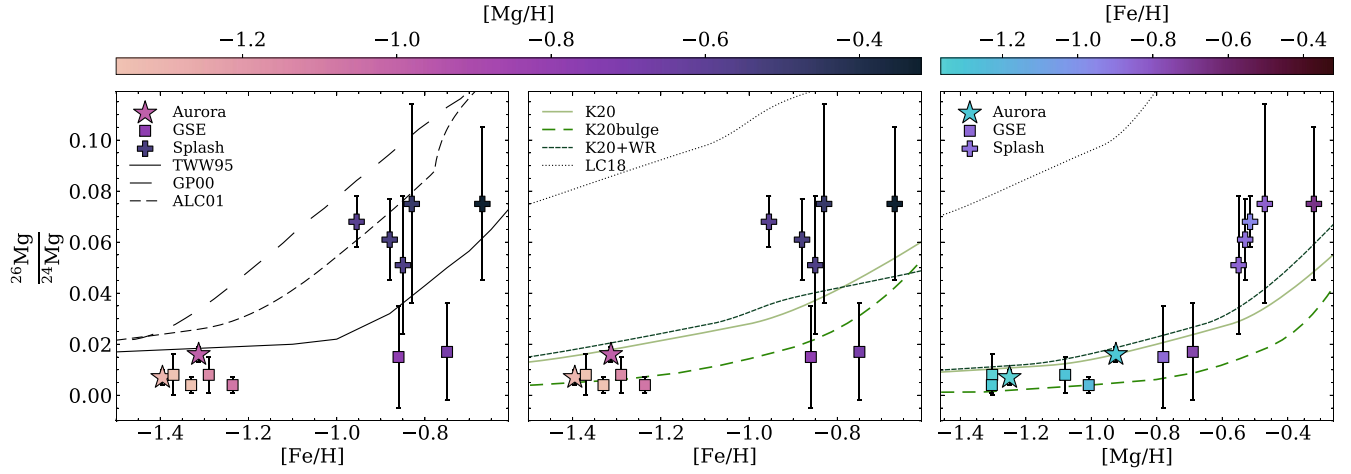

Figure 3. The correlation between ^{26}Mg/^{24}Mg and [Fe/H] (left and centre) and [Mg/H] (right). We use the same markers in Fig. 2 to represent the different MW components. In the leftmost panel, we plot the chemical evolution models from Timmes et al. (1995, TWW95, solid line), Goswami & Prantzos (2000, GP00, long-dashed line), and Alibés et al. (2001, ALC01, short-dashed line) as given in Yong et al. (2003b). In the central and rightmost panels, we plot models from Kobayashi, Tsujimoto & Nomoto (2000) and Kobayashi et al. (2020b) for the K20 (solar neighbourhood, solid light green line), the K20 bulge (bulge, long-dashed medium green line), the K20 + WR (solar neighbourhood with Wolf–Rayet stars, dark green short-dashed line), and the rotating massive stars from Limongi & Chieffi (2018, LC18, black dotted line). When plotting [Mg/H], the stars seem to follow a universal chemical evolution track, which is best reproduced by both the K20 and K20 + WR.

panel, including the same Kobayashi et al. (2020b) models from the middle panel. Our stars follow a remarkably consistent increase in ^{26}Mg/^{24}Mg, which is reproduced by all models except for the LC18 model. The Wolf–Rayet model can best reproduce the upturn in ^{26}Mg/^{24}Mg at around [Mg/H] ≈ -0.7, but still underestimates the enhancement in ^{26}Mg. This may support a slight contribution from rotating massive stars at high metallicities.

When considering the right-hand pane of Fig. 3, it appears as though the ^{26}Mg/^{24}Mg ratio follows a single chemical enrichment track. As described in Gay & Lambert (2000), the abundance of ^{25}Mg and ^{26}Mg increases with metallicity as they are predominantly a secondary species with their production relying on the abundance of the seed nucleus ^{22}Ne. However, ^{25}Mg and ^{26}Mg can occur as a *primary* process in AGB stars and rotating massive stars. In massive stars, these heavier Mg isotopes can also be produced from ^{24}Mg (Kobayashi et al. 2011). Therefore, the minor primary production of ^{25}Mg and ^{26}Mg is reflected by our low, but non-zero ^{26}Mg/^{24}Mg isotopic ratios at low [Mg/H]. As [Mg/H] increases, the ^{26}Mg/^{24}Mg ratios rise in accordance with predictions from Kobayashi et al. (2020b).

The accreted and *in situ* populations appear to follow a similar chemical track suggesting that the evolution of isotopic ratios of Mg is independent of the host galaxy, and is controlled primarily by nucleosynthesis, namely CCSNe. This hints to a universality of the

nucleosynthesis of Mg isotopes in the local Universe across cosmic time. Compared to the isotopic ratios from Gay & Lambert (2000) and Yong et al. (2003b), our improved measurements have lowered the amount of ^{26}Mg at the lower metallicity end of our isotopic ratios, making them more in line with theoretical models. Fenner et al. (2003) invoked a contribution from AGB stars to explain the scatter and elevated isotopic ratios in these previous measurements. However, the relationship between Mg isotopes and [Mg/H] found by this study indicates that the contribution of AGB stars to the Galactic inventory is small when compared to CCSNe. This is in contrast to work from Meléndez & Cohen (2007) who found that the AGB contribution in the Galactic halo increased after [Fe/H] ~ -1.5. Our results agree with more recent chemical evolution models (see fig. 18 of Kobayashi et al. 2011) and we conclude that the variation in Mg isotopes against [Fe/H] in the left and middle panels is likely due to the contribution of Fe from SNe Ia.

This interpretation is based on our small sample size, thus illustrating the need for a larger sample of high-resolution ($R > 60\,000$) and high-S/N (S/N $\gtrsim 250$) spectra to build a more comprehensive picture of Mg isotope production. Such a sample would help constrain the primary synthesis of heavy Mg isotopes, and define the metallicity at which secondary heavy Mg isotope production becomes an important factor in galactic chemical evolution.

4 CONCLUSIONS

For the first time we are able to probe stellar nucleosynthesis at the isotopic level in stars accreted from the GSE dwarf galaxy. We measure Mg isotopic ratios from high-resolution and high-S/N spectra for 13 stars using our Mg isotope code RATIO, and have assigned the kinematic membership to Aurora, Splash, or GSE components. Our results show that MW stars have a larger fraction of ^{25}Mg and ^{26}Mg at a given [Fe/H], compared to accreted dwarf galaxy stars. However, a coherent picture of the evolution of the Mg isotopes emerges when we consider the contributions from CCSNe for which the ^{26}Mg/^{24}Mg ratio appears to trace a universal chemical enrichment track. This study therefore demonstrates that while there are differences in [Mg/Fe] at a given [Fe/H] in dwarf galaxies relative to the MW, the isotopic Mg abundances suggest the universality of nucleosynthetic yields across the different star formation environments.

This letter encourages (1) further observational campaigns to comprehensively map out the isotope distribution in many more components of the MW and (2) galactic chemical evolution codes to report not only their total Mg abundances, but also the relative abundance of ^{24}Mg, ^{25}Mg, and ^{26}Mg. Our research contributes to a deeper understanding of galactic evolution, emphasizing that key isotopic ratios like ^{26}Mg/^{24}Mg maintain a uniform pattern of enrichment predominantly driven by CCSNe, irrespective of the galactic setting. These insights not only refine our understanding of chemical evolution in different galactic environments, but also pave the way for more precise observations and models of galaxy formation and evolution.

ACKNOWLEDGEMENTS

The authors thank the anonymous referee for their helpful comments that improved the clarity of this work. This research was based on observations collected at the European Southern Observatory under ESO programme 0100.D-0072(A). The authors made use of the Keck Observatory Archive, which is operated by the W. M. Keck Observatory and the NASA Exoplanet Science Institute, under contract with the National Aeronautics and Space Administration. The authors thank Professor Vasily Belokurov for constructive conversations on chemodynamic space and Dr Pamela L. Gay for sharing spectra with us. This work was supported by the Australian Research Council Centre of Excellence for All Sky Astrophysics in 3 Dimensions (ASTRO 3D) through project number CE170100013. CK acknowledges funding from the UK Science and Technology Facilities Council through grants ST/R000905/1, ST/V000632/1, and ST/Y001443/1, and also the Stromlo Distinguished Visitorship at the Australian National University. MM acknowledges the traditional custodians of the land on which the Australian National University is based, the Ngunnawal and Ngambri peoples, and pays their respects to elders past and present. This work makes use of JUPYTER notebooks (Kluyver et al. 2016) as well as the PYTHON packages NUMPY (Harris et al. 2020), MATPLOTLIB (Hunter 2007), PANDAS (The pandas development team 2020), and EMCEE (Foreman-Mackey et al. 2013).

DATA AVAILABILITY

UVES spectra are available from the ESO archive under the program reference 0100.D-0072(A). All other data, including the individual MgH line fits, are available upon reasonable request.

REFERENCES

Abdurro'uf et al., 2022, ApJS, 259, 35
Alibés A., Labay J., Canal R., 2001, A&A, 370, 1103
Bailer-Jones C. A. L., Rybizki J., Fouesneau M., Demleitner M., Andrae R., 2021, AJ, 161, 147
Barbuy B., 1985, A&A, 151, 189
Barbuy B., 1987, A&A, 172, 251
Barbuy B., Spite F., Spite M., 1987, A&A, 178, 199
Bell J. A., Gottlieb C. A., Lilley A. E., Radford H. E., 1970, ApJ, 162, L203
Belokurov V., Kravtsov A., 2022, MNRAS, 514, 689
Belokurov V. et al., 2006, ApJ, 642, L137
Belokurov V., Erkal D., Evans N. W., Koposov S. E., Deason A. J., 2018, MNRAS, 478, 611
Belokurov V., Sanders J. L., Fattahi A., Smith M. C., Deason A. J., Evans N. W., Grand R. J. J., 2020, MNRAS, 494, 3880
Bennett M., Bovy J., 2019, MNRAS, 482, 1417
Bensby T., Feltzing S., Lundström I., Ilyin I., 2005, A&A, 433, 185
Bernstein R., Shectman S. A., Gunnels S. M., Mochnacki S., Athey A. E., 2003, in Iye M., Moorwood A. F. M., eds, Proc. SPIE Conf. Ser. Vol. 4841, Instrument Design and Performance for Optical/Infrared Ground-based Telescopes. SPIE, Bellingham, p. 1694
Binney J., 2012, MNRAS, 426, 1324
Boesgaard A. M., 1968, ApJ, 154, 185
Bonaca A., Conroy C., Wetzel A., Hopkins P. F., Kereš D., 2017, ApJ, 845, 101
Bovy J., 2015, ApJS, 216, 29
Bullock J. S., Boylan-Kolchin M., 2017, ARA&A, 55, 343
Carlos M., Karakas A. I., Cohen J. G., Kobayashi C., Meléndez J., 2018, ApJ, 856, 161
Cayrel R. et al., 2004, A&A, 416, 1117
Côté B., O'Shea B. W., Ritter C., Herwig F., Venn K. A., 2017, ApJ, 835, 128
Da Costa G. S., Norris J. E., Yong D., 2013, ApJ, 769, 8
Davies E. Y., Belokurov V., Monty S., Evans N. W., 2024, MNRAS, 529, L73
Dekker H., D'Odorico S., Kaufer A., Delabre B., Kotzlowski H., 2000, in Iye M., Moorwood A. F. M., eds, Proc. SPIE Conf. Ser. Vol. 4008, Optical and IR Telescope Instrumentation and Detectors. SPIE, Bellingham, p. 534
Dodd E., Callingham T. M., Helmi A., Matsuno T., Ruiz-Lara T., Balbinot E., Lövdal S., 2023, A&A, 670, L2
Eilers A.-C., Hogg D. W., Rix H.-W., Ness M. K., 2019, ApJ, 871, 120

Fenner Y., Gibson B. K., Lee H.-c., Karakas A. I., Lattanzio J. C., Chieffi A., Limongi M., Yong D., 2003, Publ. Astron. Soc. Aust., 20, 340
Feuillet D. K., Sahlholdt C. L., Feltzing S., Casagrande L., 2021, MNRAS, 508, 1489
Fields B. D., 2011, Annu. Rev. Nucl. Part. Sci., 61, 47
Fishlock C. K., Yong D., Karakas A. I., Alves-Brito A., Meléndez J., Nissen P. E., Kobayashi C., Casey A. R., 2017, MNRAS, 466, 4672
Foreman-Mackey D., Hogg D. W., Lang D., Goodman J., 2013, PASP, 125, 306
Gaia Collaboration, 2023, A&A, 674, A1
Gallart C., Bernard E. J., Brook C. B., Ruiz-Lara T., Cassisi S., Hill V., Monelli M., 2019, Nat. Astron., 3, 932
Gay P. L., Lambert D. L., 2000, ApJ, 533, 260
Goswami A., Prantzos N., 2000, A&A, 359, 191
GRAVITY Collaboration, 2018, A&A, 615, L15
Griffith E., Johnson J. A., Weinberg D. H., 2019, ApJ, 886, 84
Griffith E. J., Weinberg D. H., Buder S., Johnson J. A., Johnson J. W., Vincenzo F., 2022, ApJ, 931, 23
Harris C. R. et al., 2020, Nature, 585, 357
Hasselquist S. et al., 2021, ApJ, 923, 172
Hawkins K., Jofré P., Masseron T., Gilmore G., 2015, MNRAS, 453, 758
Haywood M., Di Matteo P., Lehnert M. D., Snaith O., Khoperskov S., Gómez A., 2018, ApJ, 863, 113
Helmi A., White S. D. M., de Zeeuw P. T., Zhao H., 1999, Nature, 402, 53
Helmi A., Babusiaux C., Koppelman H. H., Massari D., Veljanoski J., Brown A. G. A., 2018, Nature, 563, 85
Horta D. et al., 2021, MNRAS, 500, 1385
Horta D. et al., 2023, MNRAS, 520, 5671
Hunter J. D., 2007, Comput. Sci. Eng., 9, 90
Ibata R. A., Gilmore G., Irwin M. J., 1994, Nature, 370, 194
Ji A. P. et al., 2020, AJ, 160, 181
Karakas A. I., Lattanzio J. C., 2003, Publ. Astron. Soc. Aust., 20, 279
Kluyver T. et al., 2016, in Loizides F., Schmidt B., eds, Positioning and Power in Academic Publishing: Players, Agents and Agendas. IOS Press, Amsterdam, p. 87
Kobayashi C., 2022, in Decin L., Zijlstra A., Gielen C., eds, Proc. IAU Symp. 366, The Origin of Outflows in Evolved Stars. Cambridge Univ. Press, Cambridge, p. 63
Kobayashi C., Ferrara A., 2024, ApJ, 962, L6
Kobayashi C., Tsujimoto T., Nomoto K., 2000, ApJ, 539, 26
Kobayashi C., Karakas A. I., Umeda H., 2011, MNRAS, 414, 3231
Kobayashi C., Leung S.-C., Nomoto K., 2020a, ApJ, 895, 138
Kobayashi C., Karakas A. I., Lugaro M., 2020b, ApJ, 900, 179
Leung H. W., Bovy J., 2019a, MNRAS, 483, 3255
Leung H. W., Bovy J., 2019b, MNRAS, 489, 2079
Limongi M., Chieffi A., 2018, ApJS, 237, 13
McConnachie A. W., 2012, AJ, 144, 4
McKenzie M. et al., 2024, MNRAS, 527, 7940
Mackereth J. T., Bovy J., 2018, PASP, 130, 114501
McWilliam A., Lambert D. L., 1988, MNRAS, 230, 573
Madau P., Ferguson H. C., Dickinson M. E., Giavalisco M., Steidel C. C., Fruchter A., 1996, MNRAS, 283, 1388
Mateo M. L., 1998, ARA&A, 36, 435
Matsuno T., Aoki W., Suda T., 2019, ApJ, 874, L35
Matteucci F., Greggio L., 1986, A&A, 154, 279
Meléndez J., Cohen J. G., 2007, ApJ, 659, L25
Meléndez J., Cohen J. G., 2009, ApJ, 699, 2017
Monty S., Venn K. A., Lane J. M. M., Lokhorst D., Yong D., 2020, MNRAS, 497, 1236
Moore B., Ghigna S., Governato F., Lake G., Quinn T., Stadel J., Tozzi P., 1999, ApJ, 524, L19
Myeong G. C., Vasiliev E., Iorio G., Evans N. W., Belokurov V., 2019, MNRAS, 488, 1235
Naidu R. P. et al., 2021, ApJ, 923, 92
Nissen P. E., Schuster W. J., 2010, A&A, 511, L10 (NS10)
Nissen P. E., Schuster W. J., 2011, A&A, 530, A15
Nissen P. E., Amarsi A. M., Skúladóttir Á., Schuster W. J., 2024, A&A, 682, A116
Prantzos N., Abia C., Limongi M., Chieffi A., Cristallo S., 2018, MNRAS, 476, 3432
Reggiani H., Meléndez J., 2018, MNRAS, 475, 3502
Romano D., Karakas A. I., Tosi M., Matteucci F., 2010, A&A, 522, A32
Romano D., Matteucci F., Zhang Z.-Y., Ivison R. J., Ventura P., 2019, MNRAS, 490, 2838
Schaye J. et al., 2015, MNRAS, 446, 521
Schönrich R., Binney J., Dehnen W., 2010, MNRAS, 403, 1829
Shetrone M. D., 1996, AJ, 112, 2639
Shipp N. et al., 2018, ApJ, 862, 114
Sneden C. A., 1973, PhD thesis, University of Texas, Austin
Sobeck J. S. et al., 2011, AJ, 141, 175
Spite M. et al., 2006, A&A, 455, 291
Springel V. et al., 2005, Nature, 435, 629
The pandas development team, 2020, pandas-dev/pandas: Pandas, Zenodo
Thielemann F.-K., Nomoto K., Hashimoto M.-A., 1996, ApJ, 460, 408
Thygesen A. O. et al., 2016, A&A, 588, A66
Thygesen A. O., Kirby E. N., Gallagher A. J., Ludwig H.-G., Caffau E., Bonifacio P., Sbordone L., 2017, ApJ, 843, 144
Timmes F. X., Woosley S. E., Weaver T. A., 1995, ApJS, 98, 617
Tinsley B. M., 1979, ApJ, 229, 1046
Tolstoy E., Hill V., Tosi M., 2009, ARA&A, 47, 371
Tomkin J., Lambert D. L., 1976, ApJ, 208, 436
Tomkin J., Lambert D. L., 1980, ApJ, 235, 925
Vangioni E., Olive K. A., 2019, MNRAS, 484, 3561
Venn K. A., Irwin M., Shetrone M. D., Tout C. A., Hill V., Tolstoy E., 2004, AJ, 128, 1177
Vogelsberger M. et al., 2014, Nature, 509, 177
Vogt S. S. et al., 1994, in Crawford D. L., Craine E. R., eds, Proc. SPIE Conf. Ser. Vol. 2198, Instrumentation in Astronomy VIII. SPIE, Bellingham, p. 362
Wallerstein G., 1962, ApJS, 6, 407
Wang E. X., Nordlander T., Asplund M., Lind K., Zhou Y., Reggiani H., 2022, MNRAS, 509, 1521
Weinberg D. H. et al., 2022, ApJS, 260, 32
Woosley S. E., Weaver T. A., 1995, ApJS, 101, 181
Yong D., Grundahl F., Lambert D. L., Nissen P. E., Shetrone M. D., 2003a, A&A, 402, 985
Yong D., Lambert D. L., Ivans I. I., 2003b, ApJ, 599, 1357
Yong D., Lambert D. L., Allende Prieto C., Paulson D. B., 2004, ApJ, 603, 697
Yong D., Aoki W., Lambert D. L., 2006, ApJ, 638, 1018
Yong D., Karakas A. I., Lambert D. L., Chieffi A., Limongi M., 2008, ApJ, 689, 1031
Yuan Z. et al., 2020, ApJ, 891, 39

This paper has been typeset from a TEX/LATEX file prepared by the author.